Article Pre-Print

Dynamic model of an integrated steam reforming and nuclear heat system

Leila Hoseinzade, Thomas A. Adams II*

Department of Chemical Engineering, McMaster University, 1280 Main St W,

Hamilton, Ontario, L8S 4L7, Canada

*Corresponding author: tadams@mcmaster.ca

Abstract

In this study, a dynamic and two-dimensional model for a steam methane reforming process integrated with nuclear heat production is developed. The model is based on first principles and considers the conservation of mass, momentum and energy within the system. The model is multi-scale, considering both bulk gas effects as well as spatial differences within the catalyst particles. Very few model parameters need to be fit based on the design specifications reported in the literature. The resulting model fits the reported design conditions of two separate pilot-scale studies (ranging from 0.4 to 10 MW heat transfer duty). A sensitivity analysis indicated that disturbances in the helium feed conditions significantly affect the system, but the overall system performance only changes slightly even for the large changes in the value of the most uncertain parameters.

Keyword: Dynamic modeling, Steam methane reforming, Syngas, integrated systems, nuclear heat.

1. Introduction

Syngas is an important feedstock for the production of electricity and various chemicals such as methanol, ammonia, dimethyl ether, and Fischer-Tropsch liquids. The steam methane reforming (SMR) process is a common method of producing syngas [1]. The SMR reaction is endothermic and requires high temperatures in order to achieve high conversions of methane [2]. Conventionally, the required heat for the reforming process is provided by combustion (typically using natural gas) in a furnace, through the auto-thermal reforming process, or through partial oxidation. However, there has been research into using alternative sources of providing the required high-temperature heat that could reduce the total greenhouse gas emissions (GHG) of the process [3], such as nuclear energy. For example, a study by Khojasteh-Salkuyeh and Adams [4]

examined the concept from a systems perspective for the production of Fisher-Tropsch liquids, in which helium gas was heated in a nuclear reactor to about 1200°C and then used to provide heat for natural gas reforming to produce syngas. It was determined that using nuclear heat reduces direct fossil fuel consumption for the process as a whole by about 22%, leading to carbon efficiencies of up to 72%. A follow up study examining similar ideas for methanol and dimethyl ether production found similar advantages [5]. Other studies have investigated a similar approach for using nuclear-heat-driven SMR reactions with hydrogen as the final product. Several studies were carried out in Germany and Japan on the integrated HTGR/SMR systems [6, 7, 3, 2]. In these studies, it has been demonstrated that nuclear energy is a safe, abundant and economically viable alternative to produce liquid fuels which can significantly decrease GHG emissions. In each of these cases, the key component of the system is the high temperature gas-cooled reactor (HTGR), in which a hot gas (usually helium above 800°C) provides the heat necessary to drive the endothermic SMR reaction.

The first pilot plant of an integrated SMR/HTGR was tested in 1972 in Germany [6]. This facility was called EVA-I (meaning "single splitting tube") and used a 1 MW electric heater to heat helium at 4 MPa up to 950°C in order to mimic the conditions of high-temperature helium in an actual nuclear facility. This pilot used a single tube-and-shell type configuration. The helium entered the shell, delivering heat through the wall of a single tube. The tube was filled with SMR catalyst in which natural gas and steam would be fed for the reforming reaction countercurrent to the helium. A second, helical inner tube was embedded inside of the main tube, such that the products of the SMR reaction would enter the inner tube, and reverse course to proceed in the co-current to the helium. The inner tube did not contain catalyst, and instead served strictly to provide additional heat to the catalyst zone and increase the total amount of heat transfer and thereby the methane conversion.

The original design concept used a "direct cycle" in which the helium coolant leaving the nuclear reactor directly entered the integrated SMR/HTGR. This is desirable from an efficiency point of view because the helium could be obtained at temperatures as high as 1200°C, leading to high methane conversions in the SMR. However, later studies by the Japan Atomic Energy Research Institute (JAERI) showed that it is necessary to consider an intermediate heat exchanger (IHX) and use indirect cycle. In an indirect cycle, high temperature helium leaving the nuclear reactor

does not enter the SMR/HTGR directly but instead heats a second helium stream in the IHX before returning to the nuclear reactor. The second helium stream enters the SMR/HTGR instead, which significantly enhances that safety and reliability of the process, but with the downside that the second helium stream enters at a lower temperature, making it more difficult to achieve high methane conversion.

Both EVA I and its advanced version EVA II were built, tested, and achieved their design objectives. The results from these studies were used to inform the design of a commercial scale version called the HTR-Module, with the intent of using an HTR-Module pebble bed nuclear reactor integrated with SMR, but this has not yet been constructed to the best of our knowledge [7, 2]. Later, another test facility with different design was constructed and tested by JAERI to establish a design for a larger scale integrated SMR/HTGR with 10 MW thermal output [2]. Therefore, the feasibility and satisfactory operability of the integrated SMR/HTGR system has been proven at the pilot scale.

However, many key questions must be answered before the concept can be implemented at the commercial scale. The first set of questions concerns unknowns surrounding the dynamic behaviour of the SMR/HTRG during transient conditions such as when experiencing disturbances, when starting up or shutting down the system, or when transitioning between operating modes. Understanding the dynamics of the system is critical for creating an effective control system, which is of the highest priority for nuclear-based energy systems. The second set of question concerns the unknown optimal design of the SMR/HTRG itself at commercial scale and the larger energy conversion system in which it is used. This information is critical for creating a design that is safe, reliable, and commercially viable.

Therefore, in order to answer either set of questions, a rigorous model is needed because many factors need to be considered for safety purposes, such as the avoidance of hot spots in the steel or catalysts, the non-linear effects of diffusions in complex mixtures which may have unexpected contributions during transients, and the avoidance of excessive thermal gradients during transients to avoid thermal stress on the steel tubes and shell. Due to the high temperatures involved, it is not possible to measure many of these effects directly by experiment, and therefore a sufficiently detailed model is needed. Although one prior work has examined the control system of an SMR/HTRG system [8], the study was limited to examining the controllability of the pressure

difference between the shell and the tube sides and the controllability of the other balance of plant equipment not relevant to the present study. In addition, the model used for the study was not provided in the open literature, which was based on a simplified model using transfer functions identified by experiment. As such, the model does not have predictive or generalized capability to be used in other designs

Therefore, this work focuses on the development of a dynamic model for the integrated steam reforming and nuclear heat system shown in Figure 1. In this system, hot helium from an intermediate heat exchanger flows into the shell side and transfers heat through the wall to the tube. In the tube side, process gas flows through the catalyst particles, receives heat from the hot gas in the shell, and converts to syngas. Then, hot syngas passes through an inner tube to transfer heat to the catalytic region. The model of the system is based on first principles and well-known correlations for heat and mass transfer coefficients, diffusion, and reaction kinetics. The resulting model is a set of non-linear partial differential and algebraic equations which is solved using the finite difference method. The validity of the model is tested using available pilot plant data and only a few of the model parameters need to be fitted within small regions of uncertainty. The dynamic trajectories and steady state conditions of the key variables of the system are analyzed and the effects of disturbances on the system behaviour are investigated. Finally, a sensitivity analysis on the model parameters is conducted to demonstrate the impact of parameter changes on system performance.

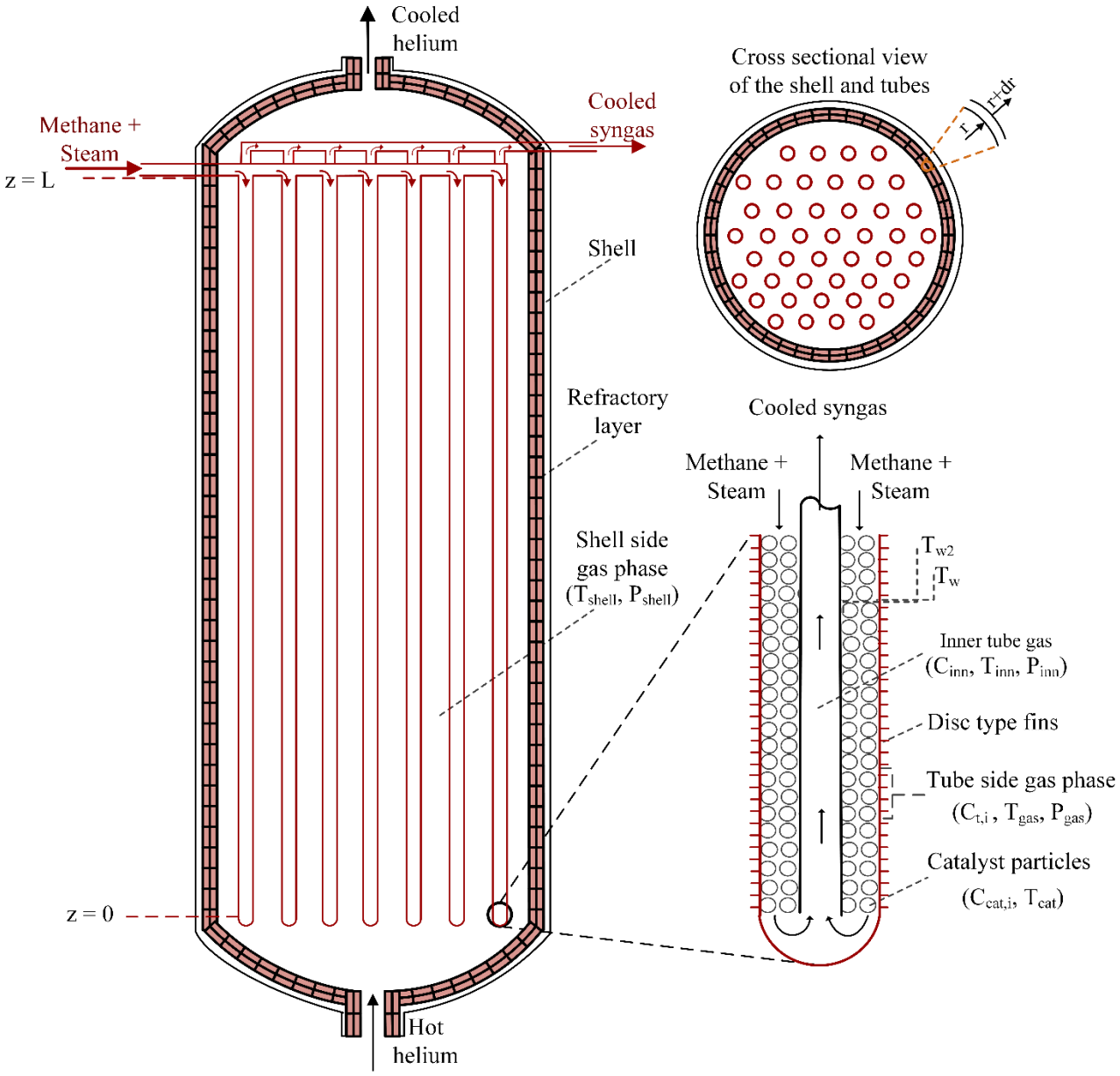

Figure 1. Schematic of integrated SMR/HTGR system with key variables of the model.

2. Model development

The proposed dynamic, heterogeneous model of integrated nuclear heat and SMR is described in this section. As shown in figure 2, the model includes seven sub-models: (1) refractory lining of the shell, (2) gas phase in the shell side, (3) outer tube wall of the steam reforming tubes, (4) gas phase in the tubes, (5) catalyst particles which are packed inside the tubes, (6) inner tube wall and

(7) gas phase in the inner tubes. It should be noted that the nuclear reactor has not been modelled in this work.

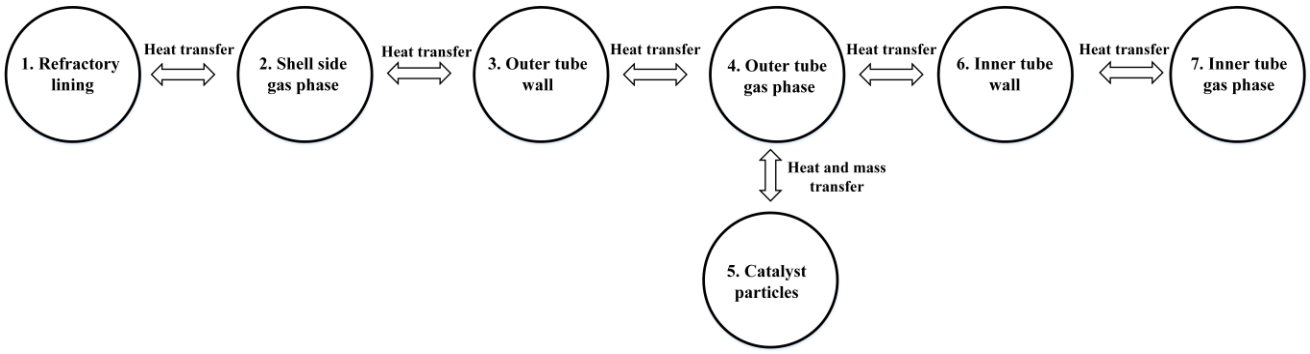

Figure 2. Integrated SMR/HTGR Sub-models.

2.1.Refractory lining

In this model, it is assumed that the refractory layer, which is used as lining to protect the shell from high temperatures, is composed of a single material. In practice, the refractory layer may be a complex layout of several different types of refractory brick such as fireclay brick, insulating brick and a castable layer [9], but the overall system performance varies very little with the type and amount of brick. Therefore, for simplicity, this model considers a single layer consisting of the average properties of the actual refractory lining layers in the energy balance equation as follows:

$$\frac{\partial T_{rfct}}{\partial t} = \frac{K_{rfct}}{\rho_{rfct} C_{p_{rfct}}} \left(\frac{\partial^2 T_{rfct}}{\partial z^2} + \frac{\partial^2 T_{rfct}}{\partial r^2} \right) \quad (1)$$

Where T_{rfct} is the refractory temperature, K_{rfct} is the refractory thermal conductivity (1.8 w/m K), ρ_{rfct} is the refractory density (2645 kg/m^3), $C_{p_{rfct}}$ is the specific heat capacity of the refractory (960 J/kg-K) [10], and r and z stand for the radial and axial positions, respectively.

To solve equation (1), four boundary conditions are required. Two of the boundary conditions are zero heat flux at the top and bottom of the refractory lining, due to the relatively small cross-sectional area [11]. These boundary conditions are given as follows:

$$\frac{\partial T_{rfct}}{\partial z}\Big|_{z=0} = \frac{\partial T_{rfct}}{\partial z}\Big|_{z=L} = 0 \quad (2)$$

The other boundary condition is the equivalency of the conductive heat with the convective and radiative heat of the gas phase at the inner wall (R_{in}) of the refractory lining and can be represented as follows:

$$-K_{rfct}\frac{\partial T_{rfct}}{\partial r}|_{r=R_{in}} = h_{shell,rfct}(T_{shell} - T_{rfct}|_{r=R_{in}}) + \sigma\epsilon_{shell}\epsilon_{rfct}(T_{shell}^4 - T_{rfct}^4|_{r=R_{in}}) \quad (3)$$

Where $h_{shell,rfct}$ is the convective heat transfer coefficient from the shell gas to the refractory lining inner wall given in the next section and T_{shell} is the shell gas phase temperature. σ is the Stefan-Boltzmann constant ($5.67 \times 10^{-8}\frac{W}{m^2\,K^4}$), $\epsilon_{shell}$and ϵ_{rfct} are the emissivity of the gas phase and refractory, respectively. ϵ_{rfct} is commonly assumed to be constant in the literature, however it changes significantly as the temperature changes. Ghouse et al. [12] proposed a correlation for ϵ_{rfct} which is given as follows:

$$\epsilon_{rfct} = -10^{-7}T_{rfct}^2 + 8 \times 10^{-5}T_{rfct} + 0.8935 \quad (4)$$

The last boundary condition denotes that the conductive heat transfer at the outer surface of the refractory is equal to the convective heat transfer at this surface. This boundary condition is given as follows:

$$-K_{rfct}\frac{\partial T_{rfct}}{\partial r}|_{r=R_o} = h_{rfct,amb}(T_{rfct|_{r=R_o}} - T_{amb}) \quad (5)$$

Where $h_{rfct,amb}$ is the convective heat transfer between the refractory outer surface and the ambient and $T_{amb}$is the ambient temperature.

2.2.Shell gas phase

This sub-model contains mass and energy balances of the helium gas flows in the shell side. The pressure drop in the shell is small (as 1 bar) and assumed to be constant [12]. The mass balance equation is given as follows:

$$\frac{\partial \rho_{shell}}{\partial t} = -\frac{\partial(\rho_{shell}v_{shell})}{\partial z} \quad (6)$$

Where ρ_{shell} is the molar density and v_{shell} is the velocity of helium gas in the shell. The boundary condition of this equation is $\rho_{shell}(t, z = 0) = \rho_{shell-inlet}$.

The energy balance equation of the shell gas phase is presented as follows:

$$\frac{\partial(\rho_{shell}H_{shell})}{\partial t} = -\frac{\partial(\rho_{shell}v_{shell}H_{shell})}{\partial z} - N_{tube}\left(q_{tube_{rad}} + q_{tube_{conv}}\right) - \left(q_{rfct_{rad}} + q_{rfct_{conv}}\right) \quad (7)$$

Where $H_{shell}$is the helium gas molar enthalpy, $N_{tube}$is the number of tubes inside the shell, $q_{tube_{rad}}$ and $q_{rfct_{rad}}$ are the radiative heat duties per volume of the gas transferred from the helium gas to each tube wall and refractory lining, respectively and $q_{tube_{conv}}$and $q_{rfct_{conv}}$ are the convective heat transferred from gas to the each tube wall and refractory lining, respectively. The enthalpy of helium gas in the shell is defined as follows:

$$H_{shell} = \Delta H_f + \int_{T_{ref}}^{T_{shell}} C_{p_{shell}} dT \quad (8)$$

Where $\Delta H_f$is the heat of formation (which is equal to zero for helium at the reference temperature T_{ref}=298.15 K) and $C_{p_{shell}}$is the specific heat capacity, which is essentially constant for helium gas in the temperature range of interest [13].

The other terms of the equation (7) are given as follows:

$$q_{tube_{rad}} = \frac{\sigma\epsilon_{shell}\epsilon_{tube}(\pi D_{t,o})\left(T_{shell}^4 - T_w^4|_{r=R_{t,o}}\right)}{A_{shell}} \quad (9)$$

$$q_{tube_{conv}} = \frac{h_{shell,w}(\pi D_{t,o})\left(T_{shell} - T_w|_{r=R_{t,o}}\right)}{A_{shell}} \quad (10)$$

$$q_{rfct_{rad}} = \frac{\sigma\epsilon_{shell}\epsilon_{rfct}(\pi D_{in})\left(T_{shell}^4 - T_{rfct}^4|_{r=R_o}\right)}{A_{shell}} \quad (11)$$

$$q_{rfct_{conv}} = \frac{h_{shell,rfct}(\pi D_{in})\left(T_{shell} - T_{rfct}|_{r=R_o}\right)}{A_{shell}} \quad (12)$$

Where ϵ_{tube} is the tube emissivity, $h_{shell,w}$is the convective heat transfer coefficient from gas to the tubes, $D_{t,o}$is the tube outer diameter, T_w is the tube wall temperature and A_{shell} is the cross-sectional area of the shell. The convective heat transfer coefficient between the shell gas phase and tube walls ($h_{shell,w}$) is given by the correlation provided by Geankopolis [1] as follows:

$$h_{shell,w} = \frac{K_{shell}}{D_{t,o}}\left(0.163\, Re_{tube} Pr_{shell}^{1/3}\right) \quad (13)$$

Where $Re_{tube} = \frac{D_{t,o} v_{shell} \rho_{mass}}{\mu_{shell}}$ is the Reynolds number over the tubes, ρ_{mass} is the mass density, μ_{shell} is the dynamic viscosity of the gas, $Pr_{shell} = \frac{C_{p_{shell}} \mu_{shell}}{K_{shell}}$ is the Prandtl number of the gas and K_{shell} is the conductive heat transfer coefficient of the shell gas.

In addition, the convective heat transfer coefficient between the shell gas phase and the refractory lining ($h_{shell,rfct}$) is given by Gneilinski as follows [10]:

$$h_{shell,rfct} = \frac{\frac{ff}{8}(Re_{rfct} - 1000) Pr_{shell}}{1 + 12.7\left(\frac{ff}{8}\right)^{\frac{1}{2}} (Pr_{shell}^{\frac{2}{3}} - 1)} \quad (14)$$

Where $ff = 0.316 Re_{rfct}^{-1/4}$ is the friction factor [10] and $Re_{rfct} = \frac{D_o v_{shell} \rho_{mass}}{\mu_{shell}}$ is the Reynolds number of the shell gas. The boundary condition of equation (7) is $T_{shell}(t, z = 0) = T_{shell-inlet}$.

2.3.Tube wall

Tube wall temperature variations are considered in radial and axial axis as follows:

$$\frac{\partial T_w}{\partial t} = \frac{K_w}{\rho_w C_{p_w}} \left(\frac{\partial^2 T_w}{\partial z^2} + \frac{\partial^2 T_w}{\partial r^2} \right) \quad (15)$$

Where K_w is the wall thermal conductivity (25.5 w/m K), ρ_w is the wall density (7940 kg/m^3) and C_{p_w} is the specific heat capacity of the wall (500 J/kg K) [14]. The tube material is Incoloy 800H and the average properties are used in the equation (15).

To solve equation (15), again four boundary conditions are required. One of the boundary conditions states that convective and radiative heat in the outer layer (R_{to}) of the tube is equal to the conductive heat transferred at that layer. This boundary condition is given as follows:

$$K_w \frac{\partial T_w}{\partial r}|_{r=R_{to}} = h_{shell,w}(T_{shell} - T_w|_{r=R_{to}}) + \sigma \epsilon_{shell} \epsilon_w (T_{shell}^4 - T_w^4|_{r=R_{to}}) \quad (16)$$

Where $h_{shell,w}$ is the convective heat transfer coefficient between the shell gas and tube outer layer, and $\epsilon_w$is the emissivity of the tube wall.

In the inner layer of the tube wall, temperature is lower and radiative heat can be neglected, thus the boundary condition at this layer (R_{ti}) can be written as:

$$K_w \frac{\partial T_w}{\partial r}|_{r=R_{ti}} = h_w(T_w|_{r=R_{ti}} - T_{gas}) \quad (17)$$

Where h_w is the convective heat transfer between the tube inner wall and the gas in the tube and given by equation (31) in the section 2.4.

At the top and bottom of the tube wall, heat flux can be assumed to be zero since the cross sectional area is small. Thus, the boundary conditions can be stated as follows:

$$\frac{\partial T_w}{\partial z}|_{z=0} = \frac{\partial T_w}{\partial z}|_{z=L} = 0 \quad (18)$$

2.4.Tube gas phase

In the tube side, steam and natural gas are mixed and converted to the syngas on the catalyst surface based on the following reactions [15]:

$$CH_4 + H_2O \rightleftharpoons CO + 3H_2 \ \left(\Delta H_{r,T_{ref}} = 206.2 \frac{kJ}{mol}\right) \quad (19)$$

$$CO + H_2O \rightleftharpoons CO_2 + H_2 \ \left(\Delta H_{r,T_{ref}} = -41.2 \frac{kJ}{mol}\right) \quad (20)$$

$$CH_4 + 2H_2O \rightleftharpoons CO_2 + 4H_2 \ \left(\Delta H_{r,T_{ref}} = 165 \frac{kJ}{mol}\right) \quad (21)$$

These reactions are highly endothermic and the required heat is provided by hot helium in the shell side. Conversion of these reactions are limited by equilibrium [11].

Key assumptions of the tube gas phase model are: ideal gas law is used for approximations [16], radial variations in the reformer tubes are negligible [17, 18] , the conditions of one tube represent the other tubes as well, a pre-reformer converts C_2^+ hydrocarbons into methane, hydrogen or carbon monoxide, so heavier-than-methane hydrocarbons are neglected in this model, and the steam/carbon ratio is high enough such that carbon deposition will not happen in the reformer [19].

The mass balance equation of gas phase in the tube is given as follows:

$$\frac{\partial C_{gas,i}}{\partial t} = \frac{\partial (C_{gas,i} v_{gas})}{\partial z} - \kappa_{gas,i} \left(C_{gas,i} - C_{cat,i}|_{r=R_p}\right)\left(\frac{a_v}{\varepsilon}\right), i = CH_4, H_2O, CO, H_2, CO_2, N_2 \quad (22)$$

Where $C_{gas,i}$ is the concentration (mol/m^3) of each component in the gas phase, v_{gas} is the interstitial velocity of the gas, $\kappa_{gas,i}$ is the mass transfer coefficient of the component i (given in the equation (24)), $C_{cat,i}|_{r=R_p}$ is the molar concentration of the component i on the catalyst surface,

$a_v = 6(1-\varepsilon)/D_p$ is the catalyst particle surface area, ε is the bed porosity and D_p is the particle diameter. The interstitial velocity of the gas is approximated by [16]:

$$v_{gas} = \frac{F_{gas}}{A_{tube}\varepsilon}\frac{RT_{gas}}{P_{gas}} \tag{23}$$

Where F_{gas} is the total inlet molar flow rate, T_{gas} is the gas phase temperature, P_{gas} is the pressure of gas, $A_{tube} = \frac{\pi}{4}(D_{ti}^2 - D_{t2,o}^2)$ is the cross sectional area of the tube and $D_{t2,o}$ is the inner tube outer diameter. Furthermore, mass transfer coefficient $\kappa_{gas,i}$ is given by [20]:

$$\kappa_{gas,i} = \frac{v_{gas_s}}{\varepsilon}\, Sc_{gas,i}^{-2/3}\left(\frac{0.765}{Re_{gas}^{0.82}} + \frac{0.365}{Re_{gas}^{0.386}}\right) \tag{24}$$

Where $Sc_{gas,i} = \mu_{gas}/\rho_{gas}\, D_{i,mix}$ is Schmidt number, $Re_{gas} = D_p\rho_{gas}v_s/\mu_{gas}$ is Reynolds number,$v_{gas_s} = v_{gas}\varepsilon$ is the superficial velocity, ρ_{gas} is the mass density of process gas, and μ_{gas} is the dynamic viscosity of the gas mixture and $D_{i,mix}$ is the diffusivity of the component i in the mixture.

Considering the counter-current configuration, the boundary condition for the equation (22) is given by:

$$C_{gas,i}(t, z = L) = C_{gas,i,inlet} \tag{25}$$

The pressure drop is computed using the Ergun equation [23] as equation (26). Due to numerical stiffness, the dynamic term in the momentum balance equation is not considered [11]. It should be noted that, in packed bed reactors pressure drop is mostly due to friction, therefore the dynamic term can be neglected [16].

$$\frac{\partial P_{gas}}{\partial z} = \frac{G}{\rho_{gas}D_p}\frac{1-\varepsilon}{\varepsilon^3}\left(\frac{150(1-\varepsilon)\mu_{gas}}{D_p} + 1.75G\right) \tag{26}$$

Where $G = \rho_{gas}v_{gas_s}$ is the mass velocity. Furthermore, the boundary condition of equation (26) is given as $P_{gas}(L) = P_{inlet}$.

In this study, the temperature in the tube side is low enough such radiative heat can be neglected. Therefore, the energy balance is written as:

$$\frac{\partial(\rho_{m,gas}H_{gas})}{\partial t} = \frac{\partial(\rho_{m,gas}v_{gas}H_{gas})}{\partial z} + q_w + q_{w_2} - q_{cat} + \sum_{i=1}^{6} q_i \tag{27}$$

Where $\rho_{m,gas}$ is the molar density, H_{gas} is the enthalpy of the gas mixture. $q_w$is the convective heat transferred from the tube wall to the gas phase (per unit volume of the gas phase), q_{w_2} is the convective heat transferred from the inner tube wall to the gas phase, q_{cat} is the convective heat transferred from the gas phase to the catalyst particles and q_i is the energy of component *i* carried from the catalyst phase to the tube gas phase or vice-versa in the form of enthalpy of the mass being transferred. The enthalpy and convective heat transfer terms are given as:

$$H_{gas} = \sum_{i=1}^{6} y_i \, H_{i,gas} \tag{28}$$

$$H_{i,gas} = \Delta H_{i,f} + \int_{T_{ref}}^{T_{gas}} C_{p,i} dT \, , \; i = CH_4, H_2O, CO, H_2, CO_2, N_2 \tag{29}$$

Where y_i is the mole fraction, $\Delta H_{i,f}$ is the formation enthalpy in the vapour state and $C_{p,i}$ is the specific heat capacity of component i in the gas phase.

$$q_w = \frac{h_w(\pi D_{ti})\left(T_w|_{r=R_{ti}} - T_{gas}\right)}{A_{tube}\varepsilon} \tag{30}$$

Where h_w is the convective heat transfer coefficient between the process gas and inner layer of the tube and D_{ti} is the inner diameter of the tube. h_w is calculated as follows [24]:

$$h_w = 0.4\frac{K_g}{D_p}\left(2.58 Re_{gas}^{\frac{1}{3}} \, {Pr_{gas}}^{\frac{1}{3}} + \; 0.094 \, Re_{gas}^{0.8} \, {Pr_{gas}}^{0.4}\right) \tag{31}$$

Where K_g is the thermal conductivity of the gas mixture, $Pr_{gas} = C_{p,mix}\mu_{gas}/K_{gas}$ is the Prandtl number and $C_{p,mix}$ is the specific heat capacity of the gas mixture.

$$q_{w_2} = \frac{h_{w_2}(\pi D_{t2,o})\left(T_{w2}|_{r=R_{t2,o}} - T_{gas}\right)}{A_{tube}\varepsilon} \tag{32}$$

Where h_{w_2} is the convective heat transfer coefficient between the process gas and outer layer of the inner tube, $D_{t2,o}$ is the outer diameter of the inner tube and T_{w2} is the inner tube wall temperature.

Convective heat transfer from the gas to the catalyst is defined as follows:

$$q_{cat} = \frac{h_{cat}a_v\left(T_{gas} - T_{cat}|_{r=R_p}\right)}{\varepsilon} \tag{33}$$

Where h_{cat} is the convective heat transfer coefficient between the gas phase and catalyst particles and T_{cat} is the catalyst temperature [25]. h_{cat} is defined as follows:

$$h_{cat} = \frac{1.37 C_{p,mix} G}{\varepsilon} \left(\frac{0.765}{Re_{gas}^{0.82}} + \frac{0.365}{Re_{gas}^{0.386}}\right) Pr_{gas}^{-2/3} \quad (34)$$

q_i is computed based on the species concentration difference between the bulk gas and catalyst surface as follows [11]:

$$if\ C_{gas,i} \geq C_{cat,i}|_{r=R_p} \ \rightarrow\ q_i = -\frac{H_{i,gas} \kappa_{gas,i} \left(C_{gas,i} - C_{cat,i}|_{r=R_p}\right) a_v}{\varepsilon} \quad (35)$$

$$if\ C_{gas,i} < C_{cat,i}|_{r=R_p} \ \rightarrow\ q_i = -\frac{H_{i,cat} \kappa_{gas,i} \left(C_{gas,i} - C_{cat,i}|_{r=R_p}\right) a_v}{\varepsilon} \quad (36)$$

Where $H_{i,gas}$ is the component i enthalpy at T_{gas} as given in equation (29) and $H_{i,cat}$ is the enthalpy of component i at T_{cat}.

The boundary condition of equation (27) is given by:

$$T_{gas}(t, z = L) = T_{gas,inlet} \quad (37)$$

2.5.Catalyst particles

The mass balance equation in the catalyst phase is given as follows:

$$\theta_{cat} \frac{\partial C_{cat,i}}{\partial t} = \frac{2}{r} D_{ei,mix} \frac{\partial C_{cat,i}}{\partial r} + \frac{\partial}{\partial r}\left(D_{ei,mix} \frac{\partial C_{cat,i}}{\partial r}\right) + r_i \rho_{cat}\ ,\ i = CH_4, H_2O, CO, H_2, CO_2, N_2 \quad (38)$$

It is assumed that particles are a homogenous mixture of solid catalyst and gas in the catalyst pores, where θ_{cat} (void fraction of catalyst particles) represents the pores' volumetric fraction in the catalyst. In the equation (38) r_i is the rate of reaction of component i, ρ_{cat} is the catalyst density and $D_{ei,mix}$ is the effective diffusivity of species i. The definition of $D_{ei,mix}$ can be found in the prior study [11]. The boundary conditions of this equation are as follows:

$$\frac{\partial C_{cat,i}}{\partial r}|_{r=0} = 0 \quad (39)$$

$$D_{ei,mix} \frac{\partial C_{cat,i}}{\partial r}|_{r=R_p} = \kappa_{gas,i} \left(C_{gas,i} - C_{cat,i}|_{r=R_p}\right) \quad (40)$$

The energy balance equation for the catalyst particles can be written as follows:

$$[(1-\theta_{cat})\rho_{cat}C_{p_{cat}} + \theta_{cat}\sum_{i=1}^{6} C_{cat,i}\, C_{p_{cat,i}}]\frac{\partial T_{cat}}{\partial t} = K_{cat}\frac{1}{r^2}\frac{\partial}{\partial r}(r^2\frac{\partial T_{cat}}{\partial r}) + \sum_{i=1}^{6} C_{p_{cat,i}} D_{ei,mix}\frac{\partial C_{cat,i}}{\partial r}\frac{\partial T_{cat}}{\partial r} + \rho_{cat}\sum_{i=1}^{6} r_i H_{i,cat} \quad (41)$$

Where $C_{p_{cat}}$ is the specific heat capacity of the catalyst particle, K_{cat} is the thermal conductivity of the catalyst particle and $C_{p_{cat,i}}$ is the specific heat capacity of component i in the catalyst phase. The boundary conditions of catalyst particles are given as follows:

$$\frac{\partial T_{cat}}{\partial r}|_{r=0} = 0 \quad (42)$$

$$[K_{cat}\frac{\partial T_{cat}}{\partial r} + \sum_{i=1}^{6} D_{ei,mix} H_{i,cat}\frac{\partial C_{cat,i}}{\partial r}]_{r=R_p} = h_{cat}\left(T_{gas} - T_{cat}|_{r=R_p}\right) - \frac{\varepsilon}{a_v}\sum_{i=6}^{6} Q_i \quad (43)$$

2.5.1. Steam reforming kinetics

The steam reforming reaction kinetics equation are presented by Xu and Froment [26] for the Ni-alumina catalyst. These kinetics have been widely accepted and cited for the steam reforming reaction. The reaction rates for equation (19)-(21) are given by equations (44)-(46), respectively.

$$r_1 = \frac{k_1}{p_{H_2}^{2.5}\, DEN^2}[p_{CH_4}\, p_{H_2O} - \frac{p_{H_2}^3 p_{CO}}{K_1}] \quad (44)$$

$$r_2 = \frac{k_2}{p_{H_2}\, DEN^2}[p_{CO}\, p_{H_2O} - \frac{p_{H_2} p_{CO_2}}{K_2}] \quad (45)$$

$$r_3 = \frac{k_3}{p_{H_2}^{3.5}\, DEN^2}[p_{CH_4}\, p_{H_2O}^2 - \frac{p_{H_2}^4 p_{CO_2}}{K_3}] \quad (46)$$

$$DEN = 1 + K_{CO}p_{CO} + K_{H_2}p_{H_2} + K_{CH_4}p_{CH_4} + \frac{K_{H_2O}p_{H_2O}}{p_{H_2}} \quad (47)$$

Where $p_i = C_{cat,i}RT_{cat}$ is the partial pressure of the corresponding species according to the ideal gas assumption. k_1, k_2 and k_3 are the reaction coefficients and defined by:

$$k_1 = 9.49 \times 10^{16}\exp\left(-\frac{28879}{T_{cat}}\right), kmol\frac{kPa^{0.5}}{kg\, h} \quad (48)$$

$$k_2 = 4.39 \times 10^{4}\exp\left(-\frac{8074.3}{T_{cat}}\right), \frac{kmol}{kPa\, kg\, h} \quad (49)$$

$$k_3 = 2.29 \times 10^{16}\exp\left(-\frac{29336}{T_{cat}}\right), kmol\frac{kPa^{0.5}}{kg\, h} \quad (50)$$

The equilibrium constants are defined as:

$$K_1 = 10266.76 \exp\left(-\frac{26830}{T_{cat}} + 30.11\right), kPa^2 \quad (51)$$

$$K_2 = \exp\left(\frac{4400}{T_{cat}} - 4.063\right) \quad (52)$$

$$K_3 = K_1 K_2 \quad (53)$$

The adsorption constants in the DEN expression are defined by:

$$K_{CH_4} = 6.65 \times 10^{-6} \exp\left(\frac{4604.28}{T_{cat}}\right), kPa^{-1} \quad (54)$$

$$K_{H_2O} = 1.77 \times 10^{3} \exp\left(-\frac{10666.35}{T_{cat}}\right) \quad (55)$$

$$K_{H_2} = 6.12 \times 10^{-11} \exp\left(\frac{9971.13}{T_{cat}}\right), kPa^{-1} \quad (56)$$

$$K_{CO} = 8.23 \times 10^{-7} \exp\left(\frac{8497.71}{T_{cat}}\right), kPa^{-1} \quad (57)$$

Based on the equations (19)-(21), reaction rates of the components can be written as:

$$r_{CH_4} = -(r_1 + r_3) \quad (58)$$

$$r_{H_2O} = -(r_1 + r_2 + 2r_3) \quad (59)$$

$$r_{CO} = r_1 - r_2 \quad (60)$$

$$r_{H_2} = 3r_1 + r_2 + 4r_3 \quad (61)$$

$$r_{CO_2} = r_2 + r_3 \quad (62)$$

$$r_{N_2} = 0 \quad (63)$$

More details on the tube model can be found in the prior work [11].

2.6.Inner tube wall

Similar to the tube model, the inner tube wall temperature variations are considered in radial and axial dimensions as follows:

$$\frac{\partial T_{w2}}{\partial t} = \frac{K_{w2}}{\rho_{w2} C_{p_{w2}}} \left(\frac{\partial^2 T_{w2}}{\partial z^2} + \frac{\partial^2 T_{w2}}{\partial r^2} \right) \quad (64)$$

Where K_{w2} is the wall thermal conductivity (28.5 w/m K), ρ_{w2} is the wall density (7880 kg/m^3) and $C_{p_{w2}}$ is the specific heat capacity of the wall (741 J/kg K) [27]. It should be noted that, the inner tube material is austenitic cast steel made up of alloy IN 519.

The boundary conditions of the inner tube wall are given as follows:

$$K_{w2} \frac{\partial T_{w2}}{\partial r}|_{r=R_{t2,o}} = h_{w2}(T_{w2}|_{r=R_{t2,o}} - T_{gas}) \quad (65)$$

The boundary condition at the inner layer of the inner tube ($R_{t2,i}$) are:

$$K_{w2} \frac{\partial T_{w2}}{\partial r}|_{r=R_{t2,i}} = h_{inn}(T_{w2}|_{r=R_{t2,i}} - T_{inn}) \quad (66)$$

Where h_{inn} is the convective heat transfer between the inner tube inner wall and the syngas.

At the top and bottom of the inner tube wall, heat flux can be assumed to be zero since the cross sectional area is small. Thus, the boundary conditions can be stated as follows:

$$\frac{\partial T_{w2}}{\partial z}|_{z=0} = \frac{\partial T_{w2}}{\partial z}|_{z=L} = 0 \quad (67)$$

2.7.Inner tube gas phase

As shown in figure 1, an inner tube is embedded inside the SMR tubes to recover heat from the hot syngas produced in the tube side. It has been shown that this helps increasing the heat transfer efficacy and methane conversion as well [2].

It should be noted that there is no reaction in the inner tube. Therefore, the mass balance equation can be written as:

$$\frac{\partial C_{inn,i}}{\partial t} = -\frac{\partial (C_{inn,i} v_{inn})}{\partial z} \quad (68)$$

Where $C_{inn,i}$ is the concentration of the component i the syngas and v_{inn} is the velocity of the gas in the inner tube and computed as follows:

$$v_{inn} = \frac{F_{gas}(0,t)}{A_{inn}} \frac{RT_{inn}}{P_{inn}} \quad (69)$$

Where $F_{gas}(0,t)$ is the exit molar flow rate of the tube, T_{inn} is the syngas temperature, P_{inn} is the pressure of the syngas in the inner tube and A_{inn} is the cross-sectional area of the inner tube.

The initial and boundary conditions of this equation are $C_{inn,i}(t, z = 0) = C_{gas,i}(0,t)$. This means that the concentration of the components at the inlet of the inner tube is the same as the tube outlet concentration.

The energy balance equation of the inner tube gas phase is given by:

$$\frac{\partial(\rho_{inn}H_{inn})}{\partial t} = -\frac{\partial(\rho_{inn}v_{inn}H_{inn})}{\partial z} - \frac{1}{A_{inn}}Q_{inn} \quad (70)$$

Where $\rho_{inn} = \sum_{i=1}^{6} C_{inn,i}$ is the molar density of the syngas in the inner tube, H_{inn} is the enthalpy of the syngas and Q_{inn} is the convective heat transferred from the syngas to the inner tube wall.

The enthalpy of the syngas in the inner tube, H_{inn} is defined as:

$$H_{inn} = \sum_{i=1}^{6} y_{inn,i}H_{inn,i} \quad (71)$$

Where $y_{inn,i}$ is the mole fraction of the component i in the gas phase and $H_{inn,i}$ is the enthalpy of the component i in the gas phase and defined in the same way as equation (29) at T_{inn} temperature.

Convective heat transferred from the gas to the inner tube wall, Q_{inn} is given by:

$$Q_{inn} = h_{inn}(\pi D_{t2,i})(T_{inn} - T_{w2}|_{r=R_{t2,i}}) \quad (72)$$

Where h_{inn} is the convective heat transfer between the inner tube gas phase and the inner tube inner wall and given by Dittus-Boelter equation [10] as follows:

$$h_{inn} = \frac{K_{inn}}{D_{t2,i}}(0.0265\, Re_{inn}^{0.8} Pr_{inn}^{0.3}) \quad (73)$$

Where K_{inn} is the thermal conductivity of the syngas (which is a function of temperature), Re_{inn} is the Reynolds number of the gas and Pr_{inn} is the Prandtl number of the syngas in inner tube.

The boundary condition for the energy balance equation is $T_{inn}(z = 0, t) = T_{gas}(0,t)$.

Similar to the shell gas phase, the pressure drop in the inner tube is small and fixed at 1 bar.

The model developed in section 2 is a set of partial differential and algebraic equations (PDAE) implemented in the gPROMS software package [28] which is an equation-oriented modelling and

simulation environment. This software uses finite difference methods (FDM) to discretize the PDEs in space. The selection and spacing of the grid points was chosen on a case-by-case basis based on error measurements and are described in later sections.

3. Model validation and parameter estimation

A survey of the literature shows that several integrated SMR/nuclear heat plants have been designed and tested for hydrogen production. As mentioned earlier, most these studies were performed by Research Center Julich, SIEMENS-INTERATOM research groups in Germany [6, 7] or by JAERI [2, 3, 29]. However, the designs developed in Germany usually use a helical or other complex geometry for the inner tubes, and thus cannot be used for validation without making significant modifications to the proposed model. However, the JAERI design uses a straight inner tube design which can be used to validate the presented model with very few modifications.

The JAERI design uses a high temperature test reactor (HTTR) to produce hydrogen from natural gas via the SMR reaction using the heat from a nuclear reactor. The safety and feasibility of the HTTR plant has been investigated by JAERI using a smaller scale test facility called the "mock-up". The mock-up reactor is $1/30^{th}$ of the size of the HTTR. Table 1 shows the key design specification of the HTTR and the mock-up reactors. As shown in the table, the mock-up reactor includes only one SMR tube inside the shell. It should be noted that, in both designs, an intermediate heat exchanger has been used between the nuclear reactor and the SMR system for safety and operability reasons [2], with helium gas chosen as the heat transfer medium in both cases. However, the temperature of the helium in the secondary cycle is lower than the primary helium cycle.

Table 1. Design specification for the High Temperature Test Reactor (HTTR) integrated with SMR. Taken from [29].

Specification	Mock-up facility	HTTR facility
Process gas conditions		
Inlet presser	4.3 MPa	4.5 MPa
Inlet temperature	450 °C	450 °C
Natural gas feed	43.2 kg/h (2.7 kmol/h)	1296 kg/h (81 kmol/h)
Outlet temperature	600 °C	580 °C
Steam to carbon ratio (S/C)	3.5	3.5
Helium gas conditions		
Inlet pressure	4.0 MPa	4.1 MPa
Inlet temperature	880 °C	880 °C
Feed rate	327.6 kg/h	8748 kg/h

Outlet temperature	650 °C	585 °C
Hydrogen product	120 Nm^3/h	4200 Nm^3/h

In the HTTR design, the temperature in the shell side is significantly lower than in conventional fossil-based SMR plants, such that radiative heat transfer is small, and the heat flux is lower as a result. To compensate for this, the HTTR uses disc-type fins around the outer surface of the tubes to increase the convective heat transfer coefficient and area. As a result, the heat transfer coefficient increases by 2.7 times and the heat transfer area increases by 2.3 times [3]. Therefore, in order to account for the effect of the fins in our model, values of the corresponding heat transfer coefficient and heat transfer area were scaled up by a factor of 2.7 and 2.3, respectively.

The key design parameters of the mock-up and HTTR pilots such as number of the tubes, tube diameter, thickness, length and material, shell diameter, inner tube diameter, thickness and material, catalyst particle size, etc., are necessary for model validation. Table 2 shows the values of these parameters wherever they has given, however as shown in the table some of these parameters have not been reported in the literature. Therefore, these missing parameters had to be estimated in order to validate the model.

Table 2. Key design parameters of the HTTR and out of pile facilities [3].

Parameter	Mock-up	HTTR
Number of tubes	1	30
Catalyst type	Ni-Alumina	Ni-Alumina
Tube material	Incoloy 800 H	Incoloy 800 H
Tube length	6.54 (m)	6.54 (m)
Tube thickness	1 cm	1 cm
Tube inner diameter	12.8 cm	12.8 cm
Inner tube thickness	-	-
Inner tube inner diameter	-	-
Catalyst particle diameter	-	-
Refractory inner diameter	16.2 cm	-
Inner tube material	-	-

The missing model parameters were estimated and their values are given in the Table 3. The parameters were estimated such that the outlet temperature of the helium gas, the outlet temperature of the syngas, and the rate of hydrogen production meet the design specifications given in table 1. Note, however, that for all of these missing parameters, the range of practical values the parameters can take is actually rather small, and do not actually have a strong influence on the reactor exit conditions. For example, the possible choices for the inner tube diameter and thickness are selected from a small subset of Japanese industrial standard sizes for alloy IN 519 pipes at relevant temperatures and pressures [30]. The diameter of the inner and outer tubes are likewise constrained to a small range of acceptable values based on geometrical limitations and reasonable spacing requirements. The average catalyst particle diameter is perhaps the most influential parameter, but again, it is limited to a very small range of possibilities given the tight spaces available. Because the parameter estimates are limited to small ranges, the estimation was carried out "by hand" via a guess-and-check approach. There were no other model parameters that needed to be estimated.

The results of the model fitting via parameters estimation are shown in Figures 3 and 4. Figure 3 indicates the model prediction of the mock-up design. The model predicts that cooled helium exits the shell at 908 K, which compares well to the actual design criteria of 923 K. On the tube side, syngas leaves the inner tube at 883 K, where the design data is 873 K. Also, the model predicts the amount of hydrogen produced to be 127 Nm^3/h, where the given design data is 120 Nm^3/h. Figure 4 shows the model prediction performance of the HTTR design; in this case, model predicts the shell outlet temperature as 869 K compared to the pilot of 853 K, and the syngas outlet temperature as 873 K, compared to the design data of 858 K. The model prediction of the hydrogen production rate is 4221 Nm^3/h and the HTTR design data for this variable is 4200 Nm^3/h. These results depict that model can predict the mock-up and HTTR plants' behaviour with high accuracy. The maximum error of the temperature prediction is 1.7% and the maximum error of the hydrogen rate production is 5.8%.

Considering the limitations in the validation of the proposed model, the results indicate that the model parameters were estimated properly and can be used to analyze and design the integrated SMR/nuclear heat systems.

Table 3. Estimated Parameters.

Parameter	Mock-up	HTTR
Inner tube thickness	0.165 cm	0.165 cm
Inner tube inner diameter	5.72 cm	5.72 cm
Catalyst particle diameter	1.2 cm	1.2 cm
Refractory inner diameter	-	0.86 m
Inner tube material	Alloy IN 519	Alloy IN 519

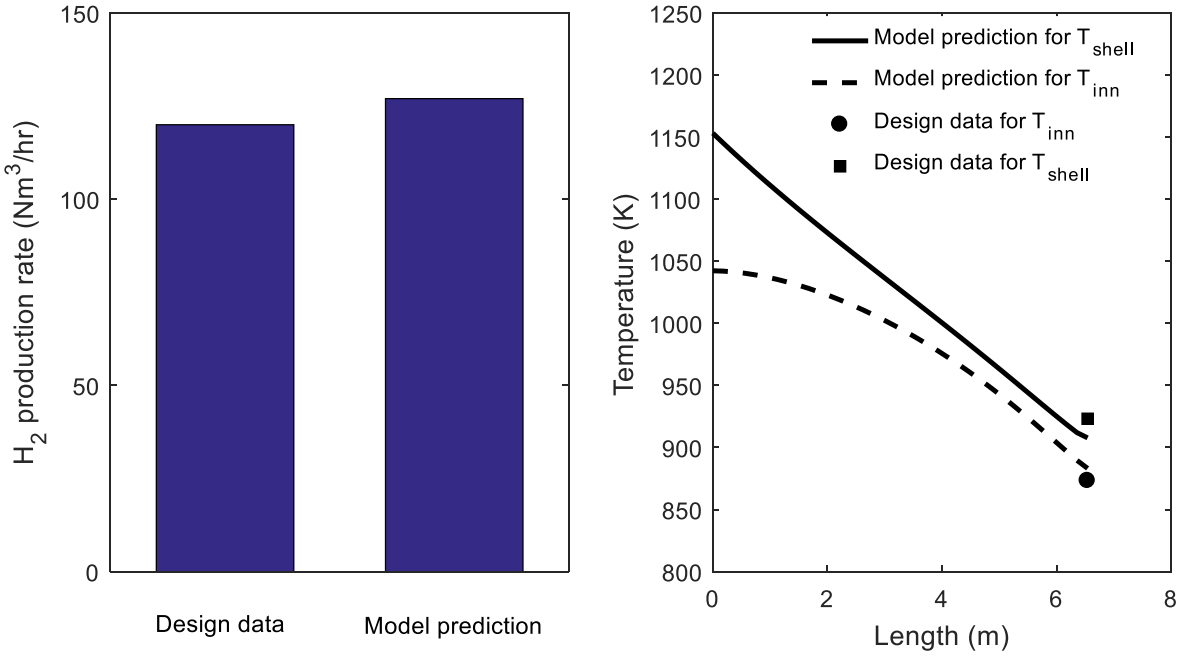

Figure 3. Model fitting using mock-up facility data.

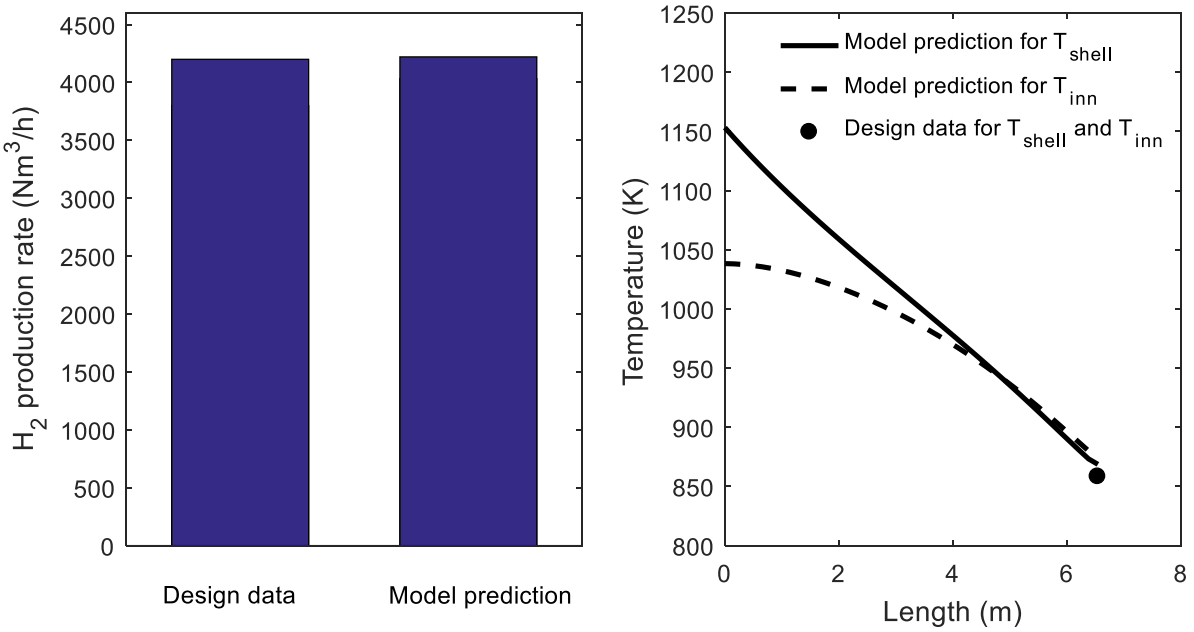

Figure 4. Model fitting using HTTR facility data.

Furthermore, choosing the number of nodes to solve the PDAE is a trade-off between the computational load and accuracy of the results. The finite differences method by its nature introduces error into the estimation of derivatives such that it does not conserve energy or mass.

Therefore, the accuracy of the results is tested based on mass and energy conservations errors within the system boundaries. These errors are defined as follows:

$$\Delta e_{m1} = \Delta m_{shell} \tag{75}$$

$$\Delta e_{m2} = m_{tube} - m_{inn} \tag{76}$$

$$\Delta e_E = \Delta E_{shell} - (\Delta E_t + \Delta E_r - \Delta E_{inn}) \tag{77}$$

Where Δe_{m1} is the overall mass balance error in the shell side and Δm_{shell} is the mass flow rate difference between the shell inlet and exit. Δe_{m2} is the mass balance error in the tube and inner tube side, m_{tube} and m_{inn} are the masses in the inlet of the outer tube and outlet of the inner tube, respectively. Δe_E is the global energy balance error, ΔE_{shell}, ΔE_t, ΔE_r and ΔE_{inn} are the energy differences between the inlet and outlet of the shell, tube, refractory and inner tube, respectively. Results show that mass balances errors are as small as 10^{-8} kg/s; however, the energy balance error changes significantly with the grid size. Table 4 shows the results of the energy balance error and CPU time at different grid sizes for the HTTR system. It can be concluded from the table that specifying axial nodes as 40, radial nodes as 60 and lateral nodes as 10 is the most efficient choice for the HTTR system considering both energy conservation error and CPU time. The error in this situation is limited to about 0.25% of the total energy transferred.

Table 4. Energy balance error vs grid size.

Number of nodes	Δe_E (MW)	CPU time (s)
Axial nodes=60, Radial nodes=50, Lateral nodes=10	0.0105	809
Axial nodes=50, Radial nodes=50, Lateral nodes=10	0.0112	635
Axial nodes=40, Radial nodes=50, Lateral nodes=10	0.0113	436
Axial nodes=40, Radial nodes=60, Lateral nodes=10	0.0091	463
Axial nodes=40, Radial nodes=40, Lateral nodes=10	0.0121	362
Axial nodes=40, Radial nodes=50, Lateral nodes=5	0.0123	394

4. Results and discussion

Although the 10 MW scale studies were useful for validation of the model, the purpose of this work is to present and study an industrial scale design for the integrated system. On such industrial-scale design is provided by SIEMENS-INTERATOM [2] to produce hydrogen via the SMR process using nuclear heat from a HTR-Module pebble bed reactor with 60 MW thermal power. The key differences between this design and HTTR facility is higher inlet temperatures and pressure of helium in the HTR-Module design. This is due to using the direct helium cycle in the HTR-Module design. In addition, the helical inner tube design in the HTR-Module rather than the straight one in the HTTR is the other key difference of these two facilities. The design specification for this system is given in Table 5.

Table 5. Design specification for an industrial scale SMR/HTGR system [2].

Specification	Large scale design
Process gas conditions	
Inlet pressure	5.6 MPa
Inlet temperature	347°C
Feed rate	34.8 kg/s
Steam to carbon ratio (S/C)	4
Helium gas conditions	
Inlet pressure	4.987 MPa
Inlet temperature	950°C
Feed rate	50.3 kg/s

The design parameters are also given in Table 6. Some of the parameters such as inner tube diameter, thickness, catalyst particle size, and the refractory diameter are not reported, those parameters except refractory inner diameter are fixed at the values estimated in the previous section. It is assumed that a triangular arrangement of tubes with the C/D ratio (which is center-to-center distance of tubes /tube outer diameter) of 2 [12] is applied in this design. Therefore, the refractory inner diameter is selected based on this assumption and the correlations and guidance presented by Kern [31] on heat exchanger design.

It should be noted that in the large scale design used in this work, the inner tubes are straight with disc-type fins on the outer surface of inner tubes to increase the convective heat transfer coefficient and area.

Table 6. Design parameters for the SMR/HTGR used in this work.

Parameter	
Reported parameters [2]	
Number of tubes	199
Catalyst type	Ni-Alumina
Tube material	Incoloy 617
Tube length	14 (m)
Tube wall thickness	1 (cm)
Tube inner diameter	12 (cm)
Estimated parameters	
Inner tube thickness	0.165 (cm)
Inner tube inner diameter	5.72 (cm)
Catalyst particle diameter	1.2 (cm)
Refractory inner diameter	2.7 (m)
Inner tube material	Alloy IN 519

4.1.Base-case Simulation results

Based on the above operating conditions and design parameters, the proposed model was used to simulate the proposed industrial design and analyze the key process variables as a function of space and time. However, because the model is complex and contains over 200,380variables and equations, *a priori* initialization is very difficult. Therefore, a workaround was used in which an initial state was given that was fictional but consistent with the model equations, such that initialization was possible *a priori*. From that fictional initial point, the simulation was run with various changes in the inlet boundary conditions that allowed the simulation to arrive at a realistic steady state. In this case, all variables were set at time zero to be either pure nitrogen on the tube side or pure helium on the shell side at 620.15 K, with the inlet boundary conditions set to pure nitrogen in the tube side and helium in the shell side flowing in at 620.15 K. This made it possible for gPROMS to successfully initialize the simulation and permit dynamic simulation to continue. The inlet feed was maintained until steady-state was reached. Then, the inlet boundary conditions were step-changed to the feed conditions given in Table 5, and the dynamic simulation continued until new steady state conditions attained. Although this final steady state condition is meaningful, the transition getting to it is not since it began from a fictional initial state. This final steady state

condition was saved and then used as the initial condition to initialize future runs of the simulation. The results are discussed next.

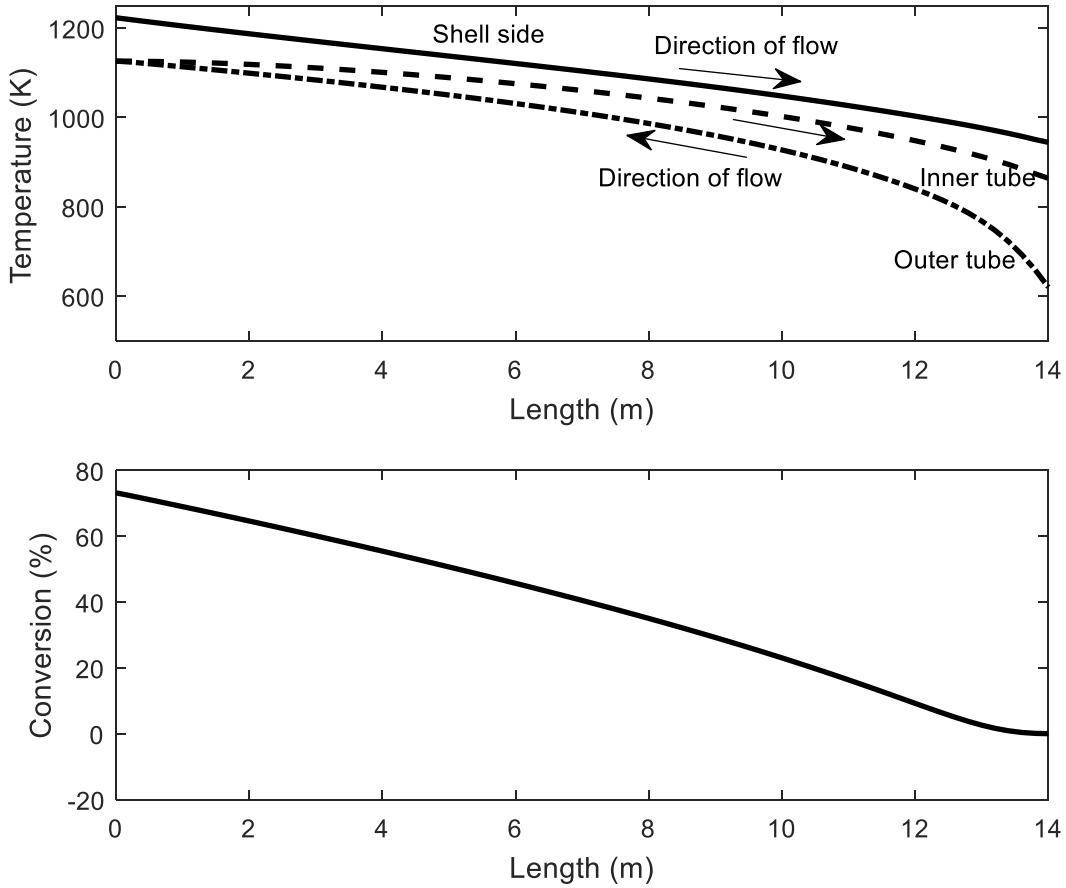

Figure 5. Temperature and conversion profiles at steady-state conditions.

The steady state performance of the integrated system is shown in Figure 5 as a function of axial variations of the shell, outer tube, and inner tube gas phase temperatures, and methane conversion in the outer tube section. It has been shown that the helium temperature in the shell drops from 1223 K in the inlet to 944 K in the shell exit, which results in 72.9 MW cooling duty. In the tube side, methane and steam mixture enter the SMR tubes at 620 K, receive heat from the shell and inner tube, convert to syngas with 73% methane conversion, then exit the tube at 1126 K. The hot syngas proceeds through the inner tube to recover its heat and exits at 864 K. Methane conversion in this system is in the range of 65%-90% which reported in the literature for SMR processes [12], but not as high as we would like. As mentioned in section 3, due to the low temperature in the shell side comparing conventional SMR processes, radiative heat transfer accounts for 5.2% of the total

heat transfer in the shell and this is one of the reasons for low conversion. In addition, high pressure (5.6 MPa) in the tubes causes lower conversion. In integrated SMR/HTGR systems, low pressure SMR cannot be applied since high pressure helium is required for the nuclear reactor.

4.2. Effect of disturbances

In order to demonstrate the impacts of disturbances on the system performance, common disturbances in the process gas (methane/steam mixture) and helium feeds such as changes in the feed temperature and steam/carbon ratio were studied.

The first disturbance investigated is a step increase of 100 K in the tube-side gas feed temperature from base-case steady state conditions. Figure 6 shows the trajectories of the shell temperature, inner tube temperature, and methane conversion at the shell and inner tube outlets (z=14 m). As a result of this change the shell outlet temperature reaches a new steady state of 959 K which increased 18 K from the previous steady state; inner tube gas outlet temperature also increases 29 K from the previous steady state. Furthermore, cooling duty drops from 72.9 MW to 68.3 MW. Methane conversion in the inner tube outlet increases only 1.2 percentage points from the previous steady state. Therefore, this disturbance does not significantly affect the overall system behaviour.

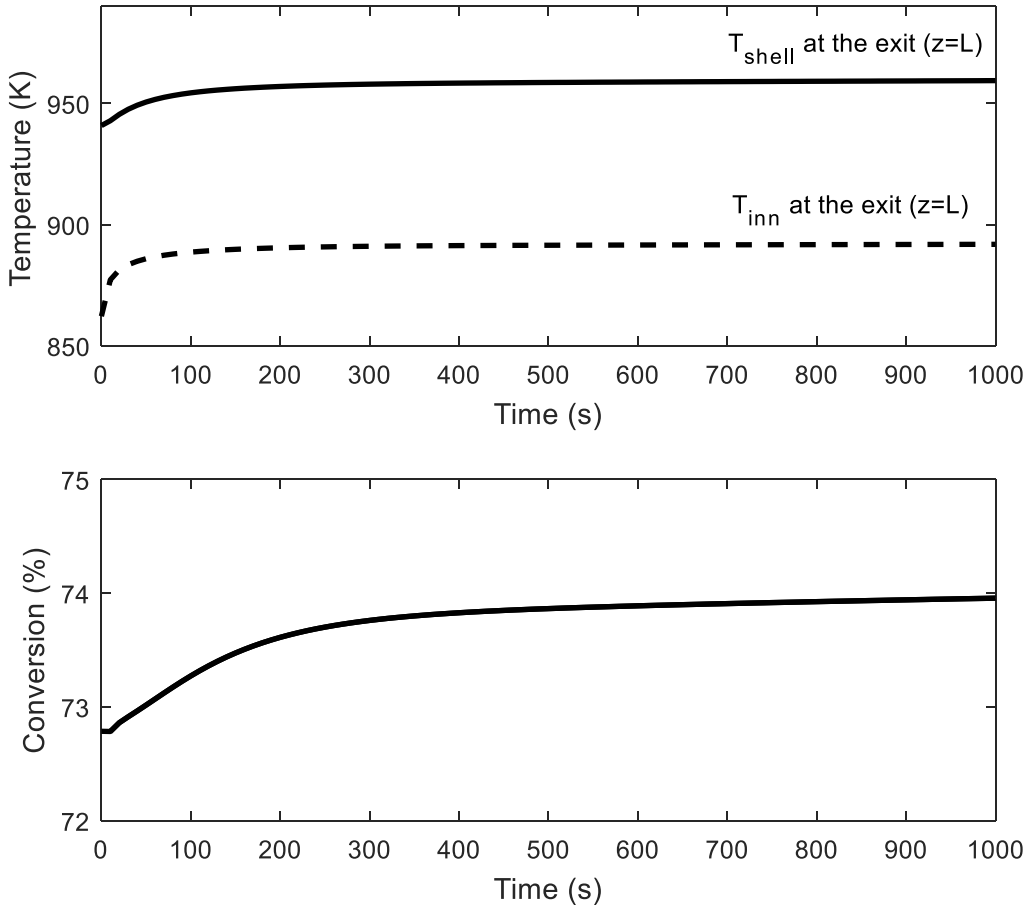

Figure 6. Effect of 100 K increase in the process gas feed at t=0 (s) on the outlet temperatures of the shell and inner tube gases and methane conversion.

The second disturbance considered in this study, is 100 K increase in the helium gas inlet temperature starting from the base case steady-state. This can happen due to an increase in the nuclear reactor temperature or feed flow rate fluctuations in the primary helium cycle. The system response to this disturbance is given in Figure 7. As shown in the figure, methane conversion significantly increases by this change. It shows a 15 percentage-point increase in the conversion from the previous steady state condition. The shell and inner tube outlet temperatures increase remarkably, also. Shell outlet temperature increased by 45 K and inner tube outlet temperature grows by 37 K from the previous steady state. Due to the larger temperature difference between the shell and tube, the cooling duty of the system also increases by 13.5 MW (18.5%).

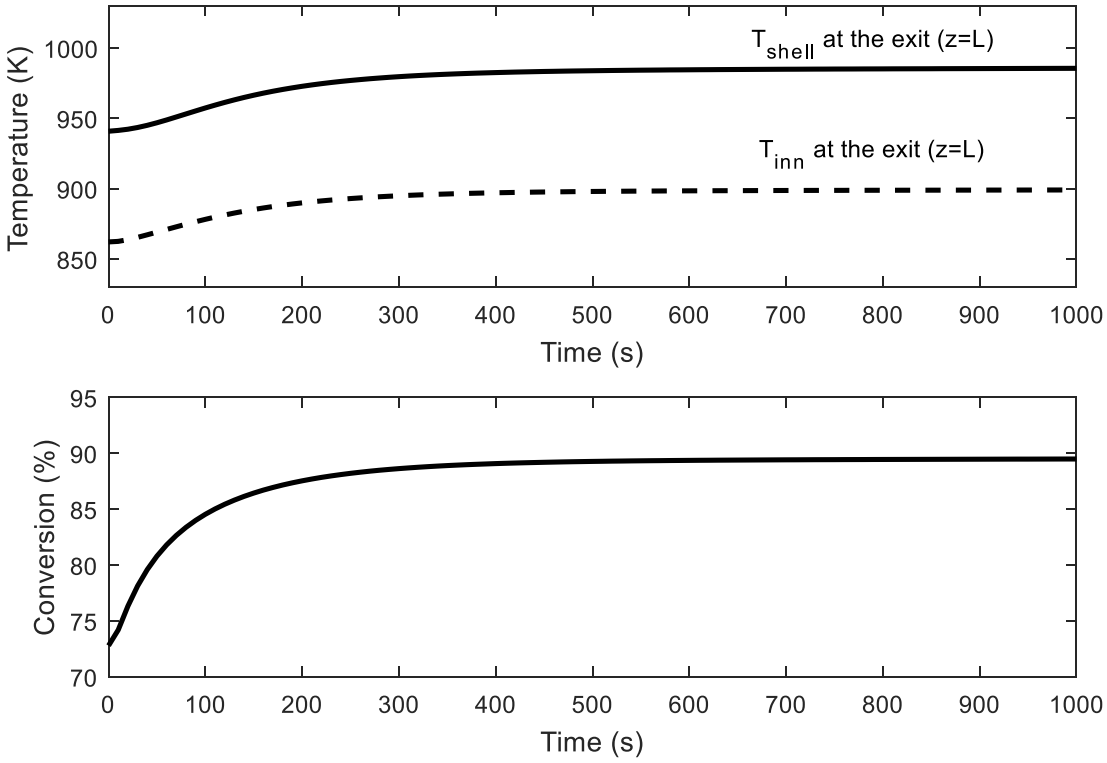

Figure 7. Dynamic response of the shell and inner tube outlet temperatures and methane conversion to the 100 K increase in the shell inlet temperature at t=0 (s).

The next disturbance investigated in this study is the impact of the change in the steam to carbon ratio (with constant total molar flow rate) on the system behavior from the base case steady-state conditions. Several step changes in the S/C ratio are introduced to the system at different times in sequence. The disturbances are steam to carbon ratio changes from 4 to 3.5 at 0 (s), from 3.5 to 3 at 2000 (s), and from 3 to 2.5 at 4000 (s). Figure 8 shows the dynamic responses of the outlet temperatures and methane conversion to these disturbances. As a result of these disturbances, the shell and inner tube outlet temperatures are change slightly from their previous steady states, with a worst-case change of only an 8 K reduction in the outlet temperatures. The cooling duty also changes only slightly as a result of the S/C disturbances. However, methane conversion shows a significant change; it changes from 0.73 to 0.67, 0.67 to 0.61 and 0.61 to 0.54, respectively, when the S/C changes from 4 to 3.5, 3.5 to 3 and 3 to 2.5. Also, methane conversion (in Figure 8) overshoots whenever a step disturbance introduced to the system. Analyzing the results indicates that diffusion and mass transfer coefficient of the methane suddenly increases due to a step

decrease in the S/C ratio. This sudden increase causes more methane consumption and, thus the overshoot in the methane conversion at that moment. Then both the diffusion and mass transfer coefficients of methane begin to decrease and result in lower methane conversion, as shown in Figure 9.

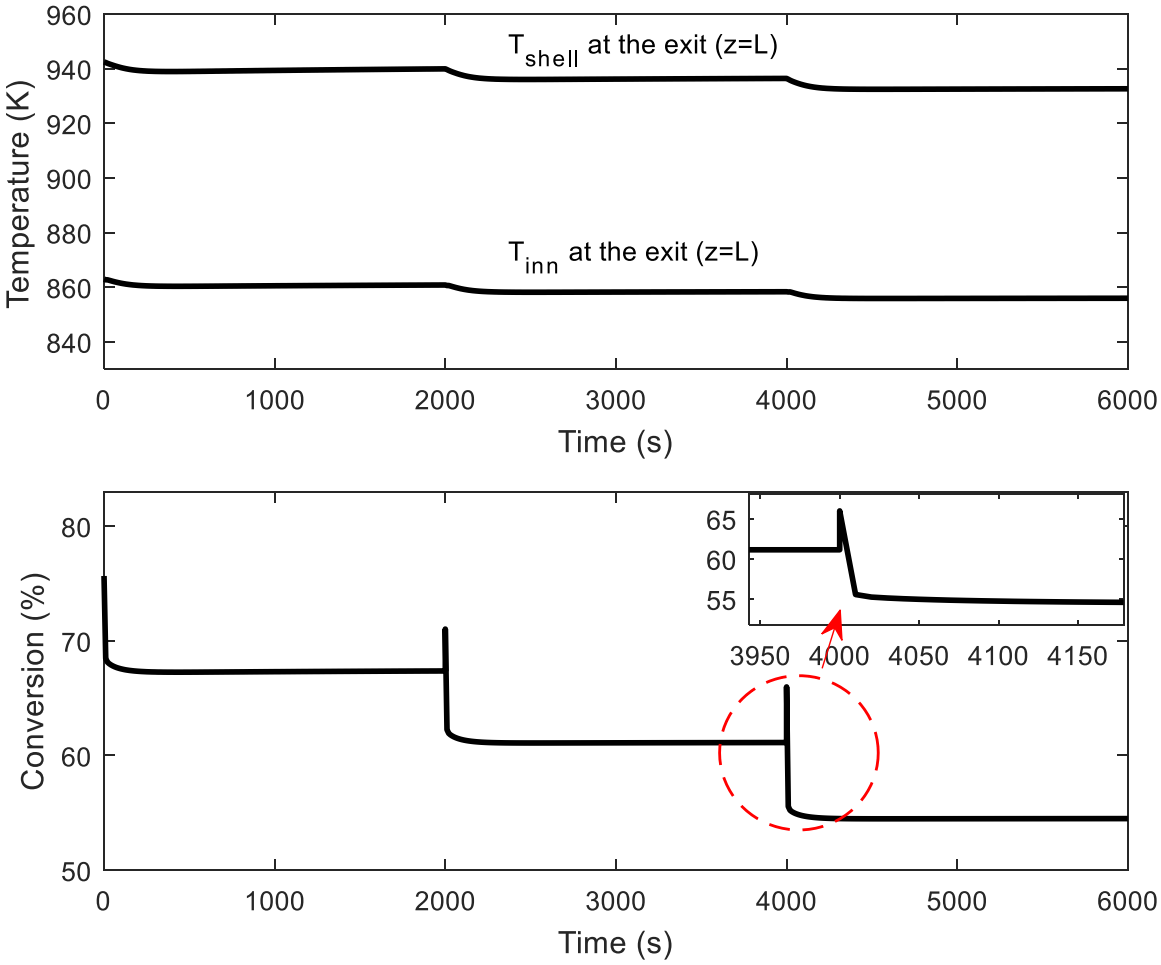

Figure 8. Dynamic response of the shell and inner tube outlet temperatures and methane conversion to the steam to carbon ratio changes from 4 to 3.5 at 0 (s), from 3.5 to 3 at 2000 (s), and from 3 to 2.5 at 4000 (s).

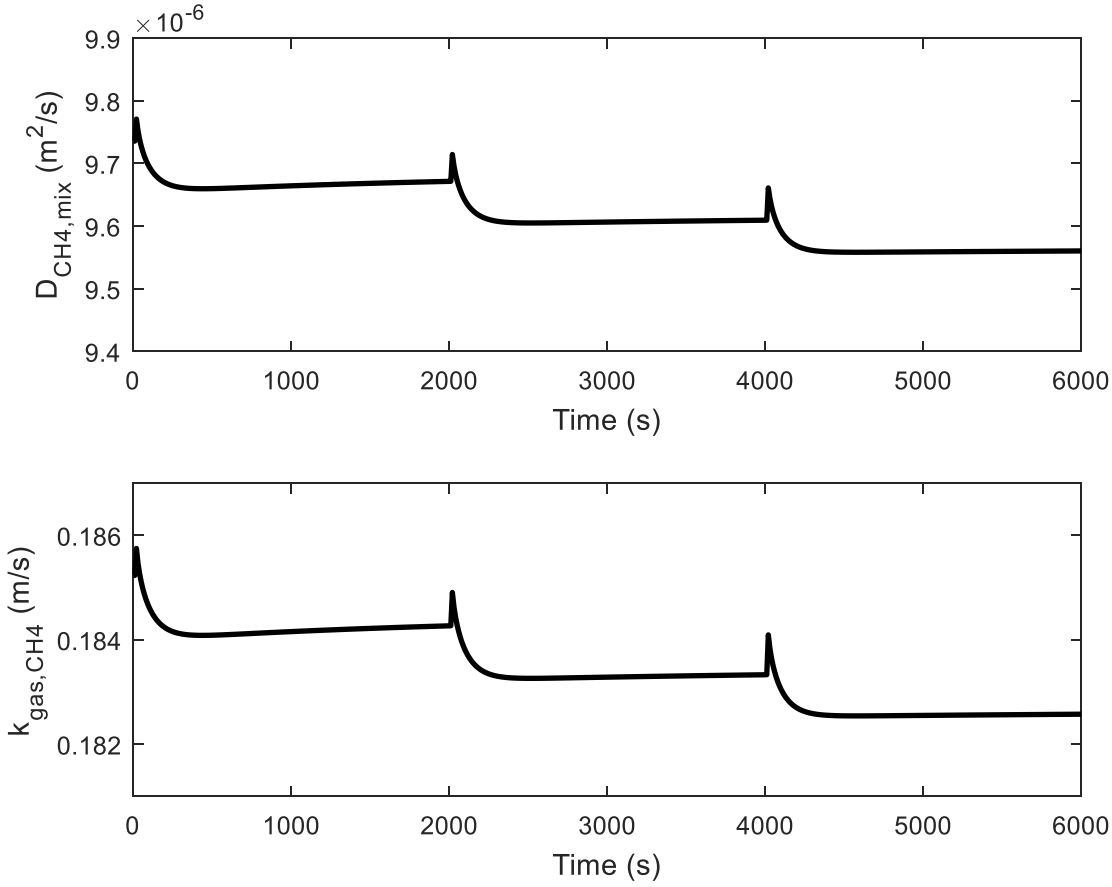

Figure 9. Methane diffusivity and mass transfer coefficients dynamic trajectories in the mixture in response to the steam to carbon ratio changes from 4 to 3.5 at 0 (s), from 3.5 to 3 at 2000 (s), and from 3 to 2.5 at 4000 (s).

4.3. Sensitivity analysis

It was noted in section 4 that some of the system parameters such as catalyst particle size, inner tube diameters, and refractory inner diameter have some uncertainty since they were estimated based on reported design data combined with engineering intuition. Even though the range of feasible values for these parameters is small, it is still important to investigate the sensitivity of the system to changes in those uncertain parameters. The system performance was analyzed for 10% and 20% changes in the nominal values of the catalyst particle size, inner tube diameters and refractory inner diameter. It should be noted that, inner tube inner and outer diameters were simultaneously changed by the same magnitude due to geometric limitations.

The sensitivity of the system is best demonstrated by the shell and inner tube exit temperatures, the methane conversion, and the cooling duty of the system, as they are the most important representatives of the integrated system behaviour. Figure 10 shows the percentage of change from

the base case values by ±10% and ±20% changes in the base case values of the parameters which are given in Table 6.

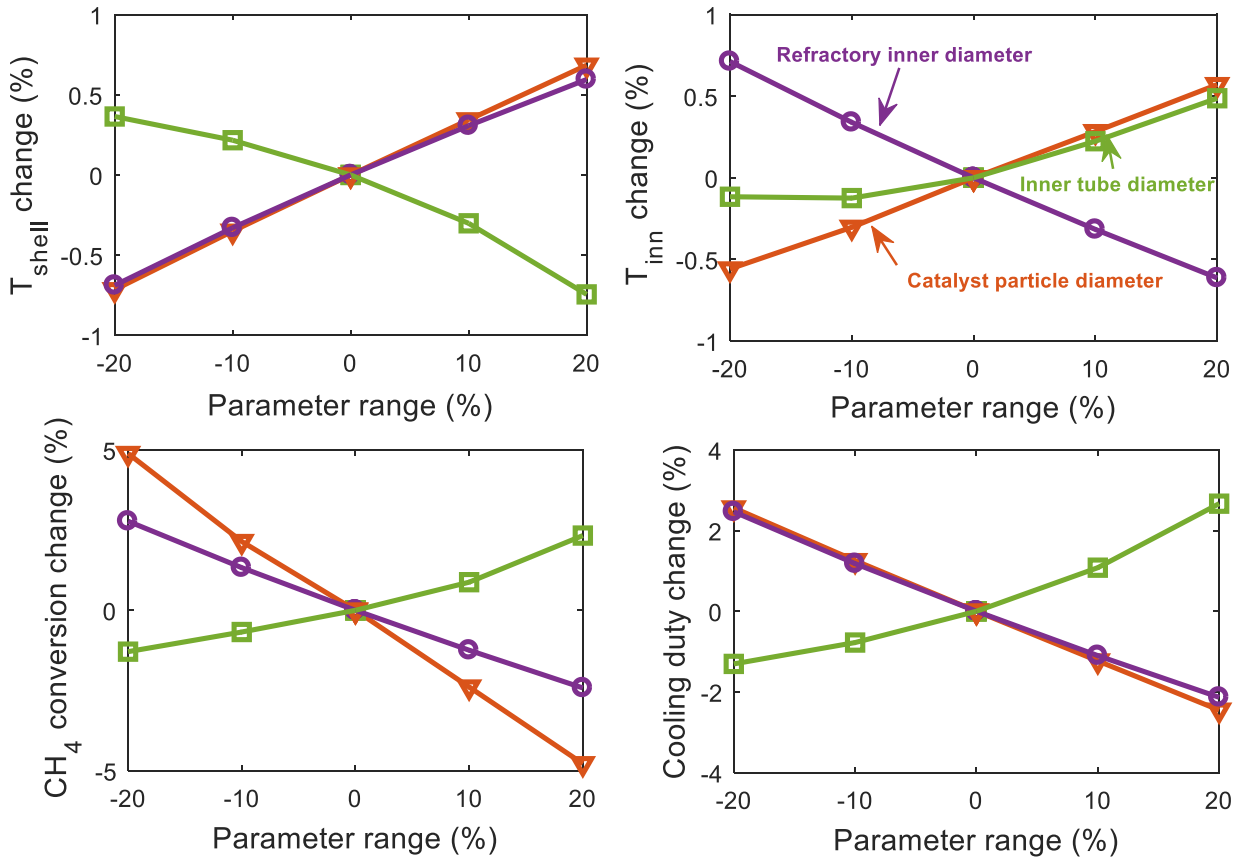

Figure 10. Sensitivity of exit temperatures of the shell and inner tube, CH_4 conversion and cooling duty of the system to some of the model parameters.

This figure indicates that a ±20% change in the value of the parameters changes the outlet temperatures of the shell and tube by at most ±0.7%, meaning that they are not very sensitive to changes in the uncertain parameters. Unlike the outlet temperatures, the methane conversion and cooling duty of the system change up to ±4.9% and ±2.7%, which depicts those variables are more sensitive to changes in those parameters, even though the overall impact is still relatively small. This indicates that the model is meaningful and useful even considering these uncertain parameters.

Generally, in most of the cases, the average catalyst particle diameter is the most influential of the uncertain parameters. The methane conversion is impacted the strongest, because smaller particle diameters can be packed together more tightly, have reduced impacts of diffusion within the

catalyst, and increase the pressure drop, all of which lead to either faster reaction kinetics and/or higher equilibrium constants. However, this does not imply that smaller particle diameters are necessarily better, because the negative effects of pressure loss at the system level can be significant in terms of both operational safety and balance-of-plant effects. The optimal particle diameter can only be determined at the systems level and is a subject of future study.

The same idea applies to the shell and tube diameters. While a smaller refractory inner diameter or greater tube diameter causes greater heat transfer from the helium gas (and thus increased methane conversion) when varied independently, shrinking the refractory inner diameter or increasing the tube diameter requires squeezing the tubes closer together, which quickly becomes impractical without removing some of the tubes. There is a lower bound on tube pitch ratio (C/D) of 1.25 for the triangular and square tube arrangements [32, 33] to allow mechanical cleaning of the tubes, and for a clear line-of-sight between the hot helium gas (for radiative heat transfer) and the tube surface, and for adequate space for gas to flow between the tubes without causing a significant pressure drop. The general conclusion here from an optimal design perspective is somewhat obvious in that the shell size and tube spacing should not be bigger than it needs to be.

5. Conclusion

This work presents, to the best of our knowledge, the first dynamic two-dimensional model for the integrated steam methane reforming and nuclear heat system. Because the model itself is based on first principles and commonly used empirical correlations of physical properties, it requires no general parameter fitting, which makes it very general and suitable for a wide variety of design applications. The model only requires information which is either known by design, or, can be readily determined experimentally at the laboratory scale, such as kinetic rate equations, common catalyst characteristics such as density and tortuosity, and basic physical property information such as heat capacity, thermal conductivity, and density. Because the model considers space-time transients within the catalyst particles themselves, it does not make use of effectiveness factors, and instead considers the transient effects of diffusion on overall reaction rates. The model was validated with two steady-state designs and predicted the output conditions of the reactors extremely well. Unfortunately, no experimental information is available on transient behaviour to use for validation of the transient portions of the model.

The model is useful for many applications such as finding the optimal design of the SMR/HTGR device and the system in which it is used, and the control of the SMR/HTGR unit which is extremely important for safety-critical systems. In particular, the model is useful for predicting phenomena which are extremely difficult to measure directly, such as the internal temperature and composition profiles inside the catalyst particles, both in steady-state or during transients. The latter is of particular importance for the design and operability of the SMR/HTGR unit because, as the results of this study showed, disturbances can lead to inverse responses caused by sudden shifts in reaction rates that could cause hot spots, cold spots, or other negative effects which are hard to measure can greatly impact long-term performance or cause safety issues.

In future work, this model will be used to help determine optimal designs for the SMR/HTGR device in the context of the entire nuclear hydrogen production system. In addition, the model will be used to develop control systems to ensure robust, safe, and stable operation. Finally, the model will be expanded to include other forms of methane reforming, such as dry reforming (reacting methane with CO_2 instead of stream) and tri-reforming (having both steam reforming and dry reforming simultaneously) by using different catalysts and system arrangements. The incorporation of CO_2 as a reagent has certain potential benefits such as CO_2 emission reduction in applications such as synthetic Fisher-Tropsch fuels or mixed alcohols synthesis.

Acknowledgment

Financial support from the Ontario Ministry of Innovation via Early Researcher Award ER13-09-213 with matching support from the McMaster Advanced Control Consortium is gratefully acknowledged. The authors would also like to acknowledge Dr. Jaffer H. Ghouse (U.S. Department of Energy, National Energy Technology Laboratory) for assistance in developing the gPROMS code.

Nomenclature

Subscripts

$rfct$	refractory
in	Refractory inner surface
o	Refractory outer surface
$shell$	shell
$conv$	convection

rad	radiation
w	Tube wall
t, o	Tube outer surface
$tube$	tube
ti	Tube inner surface
gas	Mixture of gases in the tube
cat	Catalyst phase
i	Component counter
p	particle
w_2	Inner tube wall
f	formation
mix	mixture
t_2, o	Inner tube outer surface
t_2, i	Inner tube inner surface
inn	Inner tube gas
E	Energy balance
m_1	Shell side mass
m_2	Tube side mass

Acronyms

SMR	Steam methane reforming
HTGR	High temperature gas-cooled reactor
HTTR	High temperature test reactor
GHG	Greenhouse gases
JAERI	Japan Atomic Energy Research Institute
PDAE	Partial differential algebraic equation

Greek letters

ρ	density
ϵ	emissivity
σ	Stefan-Boltzmann constant
μ	dynamic viscosity
ε	Bed porosity
π	mathematical constant
κ	Mass transfer coefficient
θ	Catalyst void fraction

References

[1] Kvamsdal HM, Svendsen HF, Olsvik O, Hertzberg T. Dynamic simulation and optimization of a catalytic steam reformer. Chem Eng Sci 1999;54(13):2697-706.

[2] Yan XL, Hino R, editors. Nuclear hydrogen production handbook. CRC Press; 2011.

[3] Inagaki Y, Nishihara T, Takeda T, Hada K, Ogawa M, Shiozawa S, Miyamoto Y. Development programme on hydrogen production in HTTR. No. IAEA-TECDOC--1210 2001.

[4] Khojasteh Salkuyeh Y, Adams II TA. Combining coal gasification, natural gas reforming, and external carbonless heat for efficient production of gasoline and diesel with CO_2 capture and sequestration. Energ Convers Manage 2013; 74: 492-504.

[5] Khojasteh Salkuyeh Y, Adams II TA. A new power, methanol, and DME polygeneration process using integrated chemical looping systems. Energ Convers Manage 2014;88:411-25.

[6] Fedders H, Harth R, Höhlein B. Experiments for combining nuclear heat with the methane steam-reforming process. Nucl Eng Des 1975;34(1):119-27.

[7] Höhlein B, Niessen H, Range J, Schiebahn HJ, Vorwerk M. Methane from synthesis gas and operation of high-temperature methanation. Nucl Eng Des 1984;78(2):241-50.

[8] Inaba Y, Ohashi H, Nishihara T, Sato H, Inagaki Y, Takeda T, Hayashi K, Takada S. Study on control characteristics for HTTR hydrogen production system with mock-up test facility: system controllability test for fluctuation of chemical reaction. Nucl Eng Des 2005;235(1):111-21.

[9] Monaghan RF, Ghoniem AF. A dynamic reduced order model for simulating entrained flow gasifiers: Part I: Model development and description. Fuel 2012;91(1):61-80.

[10] Bergman TL, Incropera FP. Introduction to heat transfer. John Wiley & Sons; 2011.

[11] Ghouse JH, Adams II TA. A multi-scale dynamic two-dimensional heterogeneous model for catalytic steam methane reforming reactors. Int J Hydrogen Energ 2013;38(24):9984-99.

[12] Ghouse JH, Seepersad D, Adams II TA. Modelling, simulation and design of an integrated radiant syngas cooler and steam methane reformer for use with coal gasification. Fuel Process Technol 2015;138:378-89.

[13] Perry RH, Green DW. Perry's chemical engineers' handbook. McGraw-Hill Professional; 1999.

[14] The story of the “INCOLOY alloys series,” from 800, through 800H, 800 HT. Special Metals Corporation. Corporation, S. M. 2004.

[15] Abbas SZ, Dupont V, Mahmud T. Kinetics study and modelling of steam methane reforming process over a NiO/Al 2 O 3 catalyst in an adiabatic packed bed reactor. Int J Hydrogen Energ 2017;42(5):2889-903.

[16] Adams II TA, Barton PI. A dynamic two-dimensional heterogeneous model for water gas shift reactors. Int J Hydrogen Energ 2009;34(21):8877-91.

[17] Pantoleontos G, Kikkinides ES, Georgiadis MC. A heterogeneous dynamic model for the simulation and optimisation of the steam methane reforming reactor. Int J Hydrogen Energ 2012;37(21):16346-58.

[18] Nandasana AD, Ray AK, Gupta SK. Dynamic model of an industrial steam reformer and its use for multiobjective optimization. Ind Eng Chem Res 2003;42(17):4028-42.

[19] Dybkjær I. Tubular reforming and autothermal reforming of natural gas—an overview of available processes. Fuel Process Technol 1995;42(2-3):85-107.

[20] Dwivedi PN, Upadhyay SN. Particle-fluid mass transfer in fixed and fluidized beds. Ind Eng Chem Proc DD 1977;16(2):157-65.

[23] Fogler HS. Elements of chemical reaction engineering. 4th ed. Upper Saddle River, NJ: Prentice Hall; 2006.

[24] Singh CP, Saraf DN. Simulation of side fired steam-hydrocarbon reformers. Ind Eng Chem Proc DD 1979;18(1):1-7.

[25] Satterfield CN. Mass transfer in heterogeneous catalysis. 1st ed. Cambridge: Massachusetts Institute of Technology Press;1970.

[26] Xu J, Froment GF. Methane steam reforming, methanation and water-gas shift: I. Intrinsic kinetics. AIChE J 1989;35(1):88-96.

[27] IN-519 cast chromium–nickel–niobium heat-resisting steel, INCO Databook1976.

[28] gPROMS, Process Systems Enterprise, 2011.

[29] Inagaki Y, Nishihara T, Takeda T, Hayashi K, Inaba Y, Ohashi H. Research and development program on HTTR hydrogen production system. International Conference on Global Environment and Advanced Nuclear Power Plants (Sept. 2003). Paper 2003 Sep 15 (Vol. 1062).

[30] JIS specification for piping. Retrieved from The engineering toolbox, http://www.engineeringtoolbox.com/jis-pipes-tubes-fittings-d_758.html.

[31] Kern DQ. Process Heat Transfer. McGraw-Hill; 1950.

[32] Mukherjee R. Effectively design shell-and-tube heat exchangers. Chem Eng Prog 1998;94(2):21-37.

[33] Sanaye S, Hajabdollahi H. Multi-objective optimization of shell and tube heat exchangers. Appl Therm Eng 2010;30(14):1937-45.